Workspace of Multi-fingered Robotic Hands Using Monte Carlo Method

Arkadeep Narayan Chaudhury[1] and Ashitava Ghosal[1]

[1]Department of Mechanical Engineering, Indian Institute of Science Bangalore
Email: {arkadeepc, asitava}@iisc.ac.in

Abstract

Multi-fingered hands enable significantly enhanced manipulation capabilities to the robot where it is attached. As a consequence, analysis, design and development of multi-fingered hands has been of continuing interest in the robotics community. In this work, we propose a probabilistic Monte Carlo based approach to obtain the workspace of a well-known multi-fingered hand, the three-fingered Salisbury hand, modeled as a hybrid parallel manipulator. It is shown that Monte Carlo method can be used to obtain the volume of the well conditioned workspace of the hybrid manipulator in $\Re^3$ and $SO(3)$. One of the obtained novel results is that with realistic constraints on the motion of the joints, the well-conditioned workspace of the hybrid manipulator is the largest when the grasped object area is approximately equal to the palm area. We also obtain and discuss the dependence of the workspace of the manipulator on it's geometry and other link and joint variables.

Keywords: Multi-fingered hand, Monte Carlo method, Well-conditioned workspace

1 Introduction

The use of multi-fingered hands in robots enable it to perform dexterous manipulation of object and thus enhance it's capabilities. Due to this reasoning several human hand inspired multi-fingered hands have been studied and built by the robotics research community. Some of the early (c.1980-90) major advances in multi-fingered hand design were robotic hands with elastic fingers ([1]), the Stanford-JPL hand ([2]), the Utah-MIT hand ([3]) and the Styx hand ([4]). In a class of works, see e.g. the works by [2] and most recently [5], researchers have explored dexterous manipulation from the context of a parallel manipulator focusing on dexterity, precision of manipulation of a given object in a given workspace by considering a lower degree of freedom (~ 6) approximation of the human hand.In this work, we study the well known three-fingered Stanford-JPL hand, originally proposed by Salisbury[2], as a hybrid parallel manipulator. The details of the modeling of the three-fingered Salisbury hand as a parallel hybrid

Table 1: Sample finger and hand segment lengths (refer figure 1 for symbols)

Hand part	Symbols	Values (mm.)
Index finger	$\{l_{11}, l_{12}, l_{13}\}$	$\{35,\ 23,\ 28\}$
Middle finger	$\{l_{21}, l_{22}, l_{23}\}$	$\{41,\ 22,\ 28\}$
Thumb	$\{l_{31}, l_{32}, l_{33}\}$	$\{45,\ 36,\ 34\}$
Palm	$\{d, h\}$	$\{13,\ 82\}$

manipulator, it's forward and inverse kinematics equations are well-known (see, for example, Ghosal [6]). In this work, we define the well-conditioned workspace of the manipulator by setting realistic constraints on the actuated and passive joints and by restricting the condition numbers of the equivalent Jacobians (relating the linear and angular velocities of the end effector separately with the joint rates) to be less than 1000 at all times. Next, using the definition of the well conditioned workspace, we formulate the problem of obtaining the well conditioned workspace of the parallel manipulator as an integration problem in the task space (in $\Re^3$ for the linear component of the motion and in $SO(3)$ for the angular component of motion of the end effector). We finally use the Monte Carlo method to evaluate the integral and obtain the workspace.

2   Description of the Stanford-JPL hand
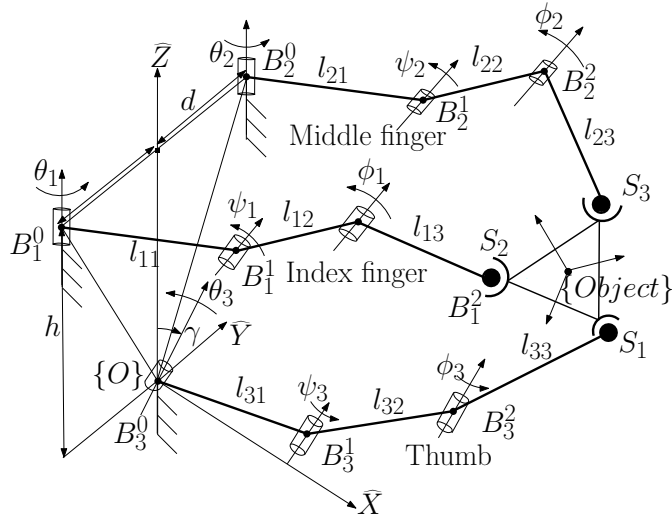
Figure 1: Schematic of the Salisbury hand (from Ghosal [6])

The kinematic model shown in figure 1 represents a three-fingered hand grasping an object. The grasping of the object is assumed to be achievable by three point contacts with friction – we have modeled them as spherical (S) joints. The manipulator, modeled as a 6-DoF hybrid parallel mechanism has been shown schematically in figure 1. In figure 1, the "gripped object" is represented by the moving platform $\{S_1, S_2, S_3\}$ connected to a "fixed base" $\{B_1^0, B_2^0, B_3^0\}$ by three 3R serial manipulators of link lengths $\{l_{i1}, l_{i2}, l_{i3}\}\ \forall i = 1, 2, 3$. The contacts between the

Table 2: Joint notations in figure 1 and maximal permissible motions

Joint center	Joint variable	Type	Value/range
B_1^0 and B_2^0	θ_1 and θ_2	Active	$-45°$ to $45°$
B_3^0	θ_3	Active	$-45°$ to $45°$
B_1^1 and B_2^1	ψ_1 and ψ_2	Active	$0°$ to $90°$
B_3^1	ψ_3	Active	$0°$ to $90°$
B_3^2	ϕ_3	Passive	$0°$ to $30°$
B_1^2 and B_2^2	ϕ_1 and ϕ_2	Passive	$0°$ to $30°$
B_3^0	γ	Fixed	$\gamma = 45°$
$S_1,\ S_2$ and S_3	$\{\xi_X^i, \xi_Y^i\}$	Passive	$\pm 45°$

gripped object and the distal ends (from the base) of the serial manipulators are modeled as 3 un-actuated "S" joints (S_1, S_2 & S_3) with three rotational degrees of freedom. It may be observed that the last "R" joint from the base towards the object shown by $\{B_1^2, B_2^2, B_3^2\}$ in figure 1 is un-actuated[1] – with this assumption the degree of freedom, by using the Grübler-Kutzbach criterion, is obtained as six. In the figure, the first joint axis of the "index" and "middle" finger are shown as parallel and the first "thumb" joint axis is at an angle of γ to the Y axis. From the figure, the position vectors of $\{B_1^0, B_2^0, B_3^0\}$ from the origin of the fixed co-ordinate system $\{O\}$ can be written as

$$^O B_1^0 = \{0, -d, h\}^T;\ ^O B_2^0 = \{0, d, h\}^T;\ ^O B_3^0 = \{0, 0, 0\}^T \tag{1}$$

and the point of contact of the fingers with the object, namely $\{S_1, S_2, S_3\}$, form the origin of $\{O\}$ can be written as

$$^O S_i =^O B_i^0 + R[\hat{Y}, \gamma_i] \begin{bmatrix} \cos(\theta_i)\left[l_{i1} + l_{i2}\cos(\psi_i) + l_{i3}\cos(\psi_i + \phi_i)\right] \\ \sin(\theta_i)\left[l_{i1} + l_{i2}\cos(\psi_i) + l_{i3}\cos(\psi_i + \phi_i)\right] \\ l_{i2}\cos(\psi_i) + l_{i3}\cos(\psi_i + \phi_i) \end{bmatrix} \tag{2}$$
$$\forall i = \{1, 2, 3\};\ \gamma = [0, 0, \pi/4]$$

Equation (2) along with the constraints imposed on the manipulator by the 3 spherical joints will be used to formulate and solve the inverse kinematics problem, obtain expressions for linear and angular velocity of the gripped object and, from the linear and angular velocity Jacobians, define the well-conditioned workspace of the manipulator. Appendices A and B briefly outline the formulation and solution of the inverse kinematics problem and the definition of the condition number of the manipulator Jacobian respectively.

2.1 Well-conditioned workspace of the manipulator using Monte Carlo method

In this section we present a brief overview of the Monte Carlo method and how it can be used to quantify and obtain a representation of the workspace of a manipulator in $\Re^3$. For a more detailed discussion on the Monte Carlo method in general, one may refer to any standard textbook of Monte Carlo method (see,

---

[1]Joints with the least motion have been chosen to be passive.

for example, Dunn and Shultis [7]). For literature on using Monte Carlo method on design and optimization of parallel manipulators one may refer to the works by Stamper at al. [8] and the references contained therein. For a comprehensive review on the usage of Monte Carlo method for obtaining the workspace volume of parallel manipulators and it's comparison with similar methods, and further implications of using it for design of parallel manipulators one may refer to [9].

We assume that the well-conditioned workspace $\mathcal{W}$, ($\mathcal{W} \in SE(3)$), of a parallel manipulator is a collection of a finite number, n, of closed sets in $SE(3)$ bounded by surfaces $\mathcal{S}_w^i$, $\forall i = 1, 2..., n$. We formulate an *in-out* function $\mathcal{F}$ for $\mathcal{S}_w^i$s which takes input of the position and orientation of the end effector of the manipulator. This function can be represented as

$$\mathcal{F}(\mathbf{X}) = \left\{ \begin{array}{ll} 1 & \text{if } \mathbf{X} \in \mathcal{W} \\ 0 & \text{if } \mathbf{X} \notin \mathcal{W} \end{array} \right\} \tag{3}$$

The inclusion(or exclusion) of a given position and orientation of the manipulator (given by $\mathbf{X} = \{x, y, z, \theta, \phi, \psi\}^T$ i.e., $\mathbf{X} \in SE(3)$ is determined by the fact that a) for a given $\mathbf{X}$ the inverse kinematics problem ($\mathcal{IK}(\mathbf{X})$ see appendix A) has real solutions, b) the active and passive joint values are within prescribed limits, and c) the manipulator Jacobian is well conditioned (see appendix B). The well-conditioned workspace is quantified by the union of all the sets $\mathcal{S}_w^i$, $\forall i = 1, 2..., n$. To obtain the well-conditioned workspace, we randomly generate N vectors $\mathbf{X}$ and evaluate $\mathcal{F}(\mathbf{X})$ for each of these points. If a randomly chosen position and orientation is in the well conditioned workspace, it is saved and at the end of the simulation, the total number of randomly generated configurations that were found to be inside the well conditioned workspace, denoted by N_{in}, is obtained. To determine the well-conditioned workspace, we define the search space $\mathcal{V}$ as the span of $\mathbf{X}$ (in Cartesian or angular coordinates) and obtain $\widehat{\mathcal{W}}$, an estimate of the well-conditioned workspace $\mathcal{W}$ of the chosen parallel manipulator as

$$\widehat{\mathcal{W}} = \frac{N_{in}}{N} \times \mathcal{V} \tag{4}$$

For a detailed discussion on the topic, one may refer to the work by Chaudhury and Ghosal [9]. Figures 2 and 3 represent the workspace of the manipulator in $\Re^3$ and angular coordinates respectively.

3   Results

Using the method described above, we can obtain separate representations of the workspace in $\Re^3$ and $SO(3)$. Figure 2 shows the representation of the workspace in $\Re^3$ as a triangulated domain, enveloping the cloud of points inside the well-conditioned workspace. Figure 3 shows the well-conditioned workspace of the parallel manipulator in $SO(3)$ as a cloud of points. The dimensions of the hand segments were taken from table 1 and the object size (circum-radius of $\triangle S_1 S_2 S_3$ in figure 1) was taken as 20mm. The volume of the obtained workspace is $1.83 \times 10^3 \text{mm}^3$. Figure 6 shows the variation of the workspace of the hand across varying hand and object sizes. For this, we considered 7 data sets (like the ones shown in table 1) from the hand dimensions of 1 female and 6 male subjects. The horizontal axis in figures 4 and 6 denotes the quantity r_{po} given by $\dfrac{\mathcal{A}_{Object}}{\mathcal{A}_{Palm}}$ where $\mathcal{A}_{Object}$ is
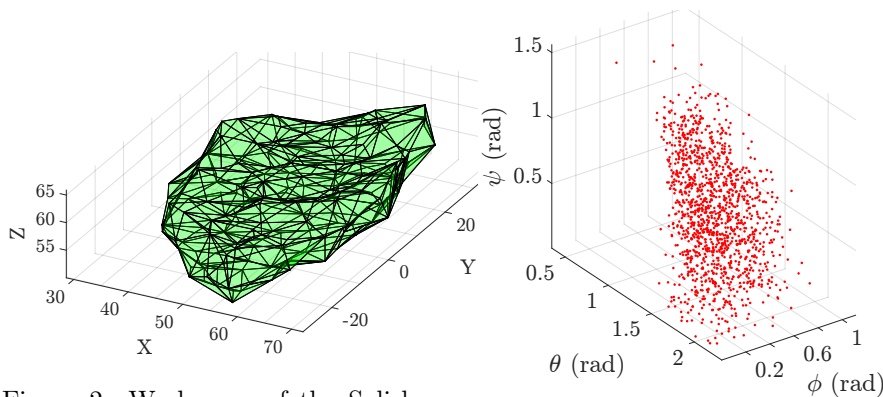
Figure 2: Workspace of the Salisbury hand

Figure 3: Angular workspace of the Salisbury hand

the area of the circum-circle of $\triangle S_1 S_2 S_3$ and $\mathcal{A}_{Palm}$ is the area of $\triangle B_1^0 B_2^0 B_3^0$ in figure 1. It may be noted that the hand workspace is the largest when the area of the palm is approximately equal to the object area – the mean r_{po}^- is found to be 1.043 with a standard deviation $\sigma(r_{po})$ of 0.05.

Since the method of obtaining the workspace is an iterative one, we demonstrate the convergence of our algorithm in figure 7. The plot shows that the algorithm gives the similar results for 40 different object sizes varying between 2mm to 40mm across 6 different executions of the algorithm. Figure 4 demonstrates that the mean r_{po}^- is independent of the upper bound on the condition number set in equation (15). To understand the dependence of the workspace of the manipulator on the geometric parameters of the manipulator we parametrize the hand as

$$\mathbf{P} = \{d, h, l_{11}, l_{12}, l_{13}, r_m = \sum_{i=1}^{3} l_{2i} / \sum_{i=1}^{3} l_{1i}, r_t = \sum_{i=1}^{3} l_{3i} / \sum_{i=1}^{3} l_{1i}\} \tag{5}$$

Next, we formulate the following optimization problem as shown below.

$$\underset{\mathbf{P}}{\text{Maximize}} \ \mathcal{W}(\mathbf{P}) \tag{6}$$

$$\text{Subject to} \quad h \times d \leq 1000, \ \sum_{i=1}^{3} l_{1i} = 80$$

$$r_m < 2, \ r_t < 2, \ l_{1i} \geq 20, \ \forall i = 1, 2, 3$$

$$d > 0, \ h > 0, \ d \leq 20, \ h \leq 80 \ \& \ d \leq 0.3h$$

The constraints imposed on the optimization problem in equation (6) are based on the 95th percentile human hand. A scaled plot of the constraint Lagrange multipliers are given in figure 5, at an optimum. The effect of the sensitivity of the hand workspace to the hand dimensions can be seen from the figure, and we can draw the following conclusions[2]:

---

[2]For a detailed discussion on constraint sensitivity analysis see Arora [10]
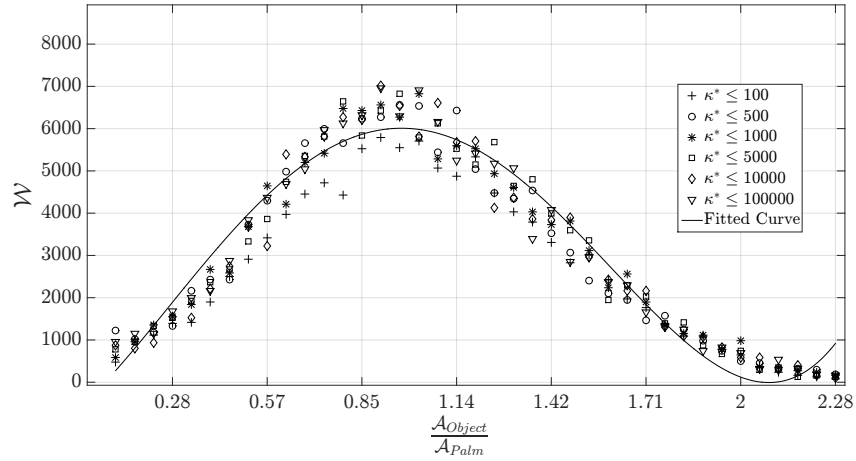
Figure 4: Independence of the result in figure 6 to upper bounds on κ^*
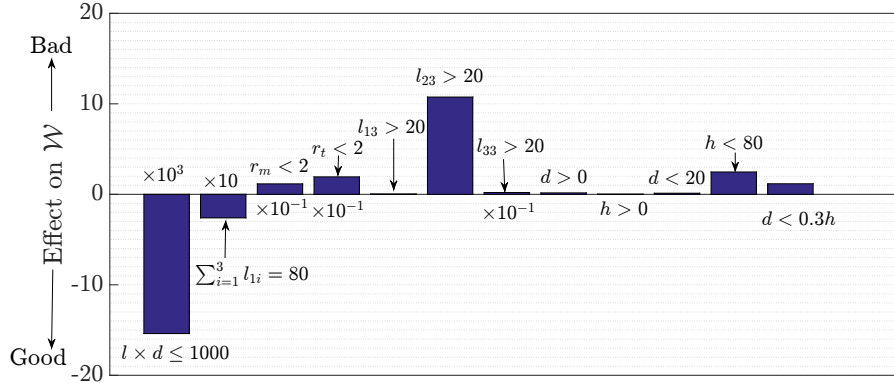
Figure 5: Scaled constraint Lagrange multipliers at an optimum

- The constraints limiting the hand size i.e., palm area and index finger length given by $l \times d < 1000$ and $\sum_{i=1}^{3} l_{1i} = 80$, have negative Lagrange multipliers associated with them, which signifies the obvious result that a *larger hand* has a larger workspace.

- From the value of the Lagrange multipliers for the constraints we observe that the workspace is more sensitive to a change in palm area than a change in finger length.

- The workspace is not very sensitive to the upper limits on r_m and r_t. Also, at an optimum we obtain $r_m = 1.1$ and $r_t = 1.35$ which are quite close to the values suggested by [11] and [12].

- The workspace is quite sensitive to lower bounds on the fingers segments, however, the workspace is not sensitive to the lower limits on d and h.

- Values of the Lagrange multipliers associated with constraints on the upper limits on d and h suggest that the workspace is equally sensitive to these

constraints.
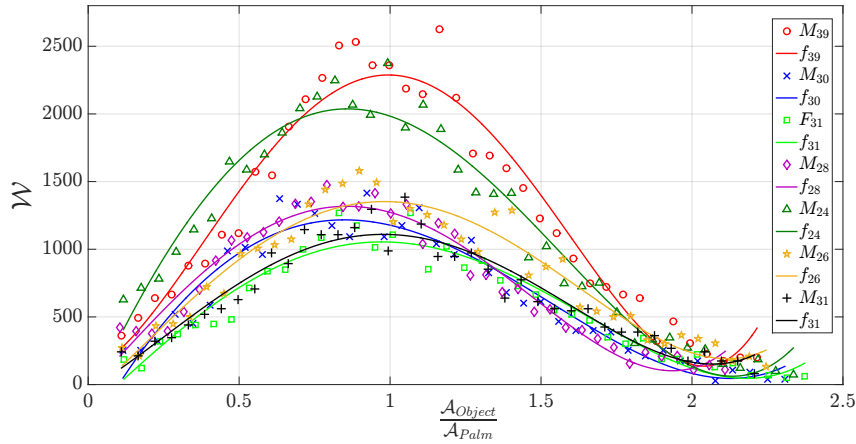
Figure 6: Variation of the workspace with varying object size
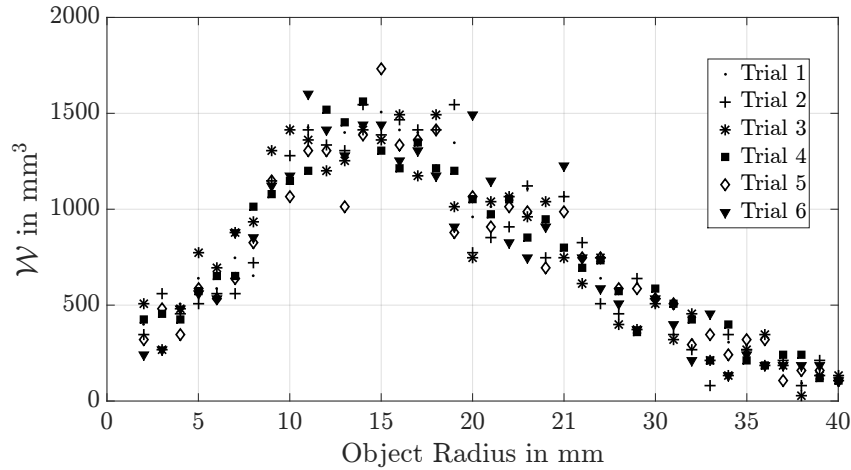
Figure 7: Convergence of algorithm over 6 trials

4   Conclusion

The current work deals with quantifying and obtaining a representation of the well-conditioned workspace of the 6-DoF hybrid parallel manipulator modeling the well-known Salisbury hand. We began by outlining the geometry of the manipulator in section 2. Following which, in section 2.1 we have outlined the use of Monte Carlo method to obtain the well-conditioned workspace of the manipulator. In section 3 we have given representations of the workspace in $\Re^3$ and $SO(3)$, and a new result indicating the the workspace of the hand is the largest when the object area is approximately equal to the palm area of the manipulator. Finally, we have outlined the dependence of the workspace of the manipulator on it's geometric dimensions.

References

[1] H. Hanafusa and H. Asada, "A robot hand with elastic fingers and its application to assembly process," in *Proc. of IFAC First Symposium on Information Control Problems in Manufacturing Technology*, pp. 127–138, 1977.

[2] J. K. Salisbury and J. J. Craig, "Articulated hands: Force control and kinematic issues," *The International Journal of Robotics Research*, vol. 1, no. 1, pp. 4–17, 1982.

[3] S. Jacobsen, E. Iversen, D. Knutti, R. Johnson, and K. Biggers, "Design of the Utah/MIT dextrous hand," in *Robotics and Automation. Proceedings. 1986 IEEE International Conference on*, vol. 3, pp. 1520–1532, IEEE, 1986.

[4] R. M. Murray and S. S. Sastry, "Control experiments in planar manipulation and grasping," in *Robotics and Automation, 1989. Proceedings., 1989 IEEE International Conference on*, pp. 624–629, IEEE, 1989.

[5] J. Borràs and A. M. Dollar, "Dimensional synthesis of three-fingered robot hands for maximal precision manipulation workspace," *The International Journal of Robotics Research*, vol. 34, no. 14, pp. 1731–1746, 2015.

[6] A. Ghosal, *Robotics: Fundamental Concepts and Analysis*. Oxford University Press, 2006.

[7] W. L. Dunn and J. K. Shultis, *Exploring Monte Carlo Methods*. Elsevier, 2011.

[8] R. E. Stamper, L.-W. Tsai, and G. C. Walsh, "Optimization of a three DOF translational platform for well-conditioned workspace," in *Robotics and Automation, 1997. Proceedings., 1997 IEEE International Conference on*, vol. 4, pp. 3250–3255, IEEE, 1997.

[9] A. N. Chaudhury and A. Ghosal, "Optimum design of multi-degree-of-freedom closed-loop mechanisms and parallel manipulators for a prescribed workspace using monte carlo method," *Mechanism and Machine Theory*, vol. 118, pp. 115–138, 2017.

[10] J. Arora, *Introduction to Optimum Design, Chapter 4, pp 154-157,*. Academic Press, 2004.

[11] R. M. White, "Comparative anthropometry of the hand," tech. rep., DTIC Document, 1980.

[12] J. T. Manning, "Sex differences and age changes in digit ratios: Implications for the use of digit ratios in medicine and biology," in *Handbook of Anthropometry*, pp. 841–851, Springer, 2012.

Appendices

A Inverse kinematics problem solution [6]

For a given position vector of the point S_1, (see figure 1), the expressions of the X, Y and Z coordinates of the point S_1 are given as the rows of equation (2). From which, by simplifying $X^2 + (Y + d)^2 + (Z - h)^2$ we can obtain the expression with only ϕ_1, given in equation (7).

$$4l_{11}^2(l_{12}^2 + l_{13}^2 + 2l_{12}l_{13}\cos(\phi_1)) = C_1^2 + 4l_{11}C_2^2 \tag{7}$$

where $C_1 \equiv C_1(l_{11}, l_{12}, l_{13}, d, h, \phi_1)$ and $C_2 = h - Z$. Substituting $\cos(\phi_1)$ with its tangent half angle equivalent in equation (7) we can obtain a quadratic expression for ϕ_1. The angle ψ_1 can be solved from the eliminant obtained by using Sylvester's dialytic method and θ_1 is obtained as $\theta_1 = \text{atan2}(Y+d, X)$. The inverse kinematics problem for the middle finger and the thumb can be solved in a way similar to index finger shown above.

B Definition of condition number

The position vector of the center of the object in figure 1 is given by,

$$^OP_{Obj} = \frac{1}{3}\sum_{i=1}^{3} {}^OS_i \tag{8}$$

and the orientation of the top platform with the base may be given as in

$$^O[R]_{Obj} = \left[\begin{array}{ccc} \dfrac{^OS_1 - ^OS_2}{|^OS_1 - ^OS_2|} & \hat{Y} & \dfrac{(^OS_1 - ^OS_1) \times (^OS_1 - ^OS_3)}{|(^OS_1 - ^OS_1) \times (^OS_1 - ^OS_3)|} \end{array} \right] \tag{9}$$

where $\hat{Y}$ is obtained by the cross product of the third and first column of the matrix in equation (9). The 3 constraint equations ensuring that the distance $||S_i - S_j||$, $\{i, j\} \in [1, 2, 3], i \neq j$, are always constant, may be differentiated to obtain equation (10).

$$[\mathbf{K}(\theta, \phi)]\{\dot{\theta}\} + [\mathbf{K}^*(\theta, \phi)]\{\dot{\phi}\} = 0 \tag{10}$$

It is easily seen that $[\mathbf{K}^*]$ is a square matrix of dimension 3×3. Equation (10) can be solved for $\dot{\gamma}$, given $\det(\mathbf{K}^*) \neq 0^3$, and we can obtain $\dot{\phi} = -[\mathbf{K}^*(\theta, \phi)]^{-1}[\mathbf{K}(\theta, \phi)]\dot{\theta}$. Differentiating equations (8) and (9) with respect to time we obtain the expressions for the linear and angular velocities of the manipulator and these can be written as

$$^0V_{Obj} = [\mathbf{J}_V]\{\dot{\theta}\} + [\mathbf{J}_V^*]\{\dot{\phi}\} \tag{11}$$

$$^0\omega_{Obj} = [\mathbf{J}_\omega]\{\dot{\theta}\} + [\mathbf{J}_\omega^*]\{\dot{\phi}\} \tag{12}$$

---

[3]In the simulation, it was ensured that $\det(\mathbf{K}^*) \neq 0$ and the condition number of $\mathbf{K}^*$ was $\leq 10^4$ at all points inside the obtained workspace.

Following [6] and using equations (10) to (12) we define the square, nonsingular, equivalent Jacobian matrices for both linear and angular velocity parts as

$$\mathbf{J}_{eqv}^{V} = (\mathbf{J}_V - \mathbf{J}_V^*[\mathbf{K}^*]^{-1}[\mathbf{K}]) \tag{13}$$

$$\mathbf{J}_{eqv}^{\omega} = (\mathbf{J}_\omega - \mathbf{J}_\omega^*[\mathbf{K}^*]^{-1}[\mathbf{K}]) \tag{14}$$

The equivalent, dimensionless condition number of Jacobian for the manipulator, undergoing both linear and angular motions are given as κ_V and κ_ω for $\mathbf{J}_{eqv}^{V}$ and $\mathbf{J}_{eqv}^{\omega}$ respectively where we find the 2-norm condition number of a matrix $\mathbf{A}$ as $\kappa_A =\parallel \mathbf{A} \parallel_2 \parallel \mathbf{A}^{-1} \parallel_2$. To ensure that a given configuration of the end effector is well conditioned we ensure that

$$\max\{\kappa_V, \kappa_\omega\} \leq \kappa^* \tag{15}$$

where κ^* is chosen as 1000.